Journal of
Materials Chemistry B

PAPER

View Article Online
View Journal | View Issue

Cite this: J. Mater. Chem. B, 2016, 4, 2614

A photostable AIEgen for nucleolus and mitochondria imaging with organelle-specific emission†

Chris Y. Y. Yu,‡[ab] Weijie Zhang,‡[ab] Ryan T. K. Kwok,[ab] Chris W. T. Leung,[ab] Jacky W. Y. Lam[ab] and Ben Zhong Tang*[abc]

Received 4th February 2016,
Accepted 8th March 2016

DOI: 10.1039/c6tb00319b

www.rsc.org/MaterialsB

Dynamic visualization of the morphology of membrane-bound organelles offers useful insights for studying various intracellular activities. Fluorescent probes with superior specificity and photostability are desirable for long-term tracking of these processes. In this work, we present the design and synthesis of an α-cyanostilbene derivative, abbreviated as ASCP, with the aggregation-induced emission (AIE) characteristic, and its application in cell imaging. ASCP can simultaneously label mitochondria and nucleolus in live cells with distinct fluorescence, which is demonstrative of a single molecule with dual-colour organelle imaging.

1. Introduction

Nucleolus is the key structure in the nucleus. It serves as the site for ribosome synthesis and RNA assembly,[1] and is thus closely related to the cell growth and proliferation. RNA assembly occurs during the late telophase and disassembles in mitosis after the interphase.[2–5] The details of dynamic nucleolar RNA distribution and localization throughout the cell cycle, however, have not been fully understood as dye molecules for specific labelling of the RNA in live cells are rare.[6,7] Recent reports also found that the morphology of nucleolus is associated with several neurodegenerative disorders such as Parkinson's disease.[8,9] Thus, the development of new luminescent materials for RNA imaging in live cells is one of the hot research topics in materials science.

SYTO RNASelect is a commercial RNA-selective fluorescent probe that is commonly used for tracking the morphology change of nucleolus.[10] It is virtually non-fluorescent but exhibits bright green fluorescence when bound to RNA. However, its performance degrades easily due to its low photostability and small Stokes shift (absorption/emission maximum: 490/530 nm). Thanks to the enthusiasm of scientists, a variety of RNA probes have recently been developed based on oligonucleotides,[11] the mechanisms of fluorescence resonance energy transfer (FRET),[12] dual-labelled oligonucleotide hairpin,[13] dual FRET molecular beacons[14] and autoligation as well as fluorescent proteins.[15] Unfortunately, some of them are prepared through complicated synthetic procedures and involve expensive production costs. Meanwhile, microinjection is sometimes required in cell staining, which is invasive and may cause cell damage and an uneven distribution of dye molecules. On the other hand, small organic fluorophores are promising alternatives for live cell nucleolus imaging.[16–18] For example, Chang *et al.* and Ge *et al.* designed and synthesized a series of styryl dyes and hemicyanine derivatives, respectively, for visualizing the intracellular nucleolus with different emissions.[19–21]

Mitochondria are known as the powerhouses of the cell. In addition to supplying cellular energy, mitochondria also play a vital role in many metabolic tasks such as regulation of membrane potential and apoptosis-programmed cell death. The morphology of mitochondria is controlled by a set of proteins. Any unexpected disruption of mitochondrial membrane is implicated in several human diseases including degenerative diseases, such as Parkinson's and Alzheimer's diseases.[22,23] Various types of fluorescent probes that can selectively illuminate the mitochondria have been developed in order to monitor the morphology change of mitochondria and study these processes. Owing to the fact that the light emissions of these probes are often

[a] HKUST Shenzhen Research Institute, No. 9 Yuexing 1st Road, South Area, Hi-tech Park, Nanshan, Shenzhen 518057, China. E-mail: tangbenz@ust.hk
[b] Department of Chemistry, Hong Kong Branch of Chinese National Engineering Research Center for Tissue Restoration and Reconstruction, Institute for Advanced Study, Division of Biomedical Engineering, Division of Life Science, State Key Laboratory of Molecular Neuroscience, Institute of Molecular Functional Materials, The Hong Kong University of Science and Technology, Clear Water Bay, Kowloon, Hong Kong, China
[c] Guangdong Innovative Research Team, SCUT-HKUST Joint Research Laboratory, State Key Laboratory of Luminescent Materials and Devices, South China University of Technology, Guangzhou 510640, China

† Electronic supplementary information (ESI) available: Characterization of ASCP and intermediates, and chemical structures of phospholipids used in this study. See DOI: 10.1039/c6tb00319b

‡ These authors contributed equally to this work.

weakened by aggregate formation, they are generally used at very low concentrations. However, such a small number of dye molecules are quickly photo-bleached under continuous light irradiation from the fluorescence microscope. Thus, these fluorescent probes are not capable of observing the dynamic morphology change of mitochondria for a prolonged period of time.

To achieve long-term cellular tracking, alternative systems with higher photostability are thus in urgent demand. Recently, some luminogens have been found to exhibit a phenomenon of aggregation-induced emission (AIE). These molecules are non-fluorescent in dilute solutions but emit strong light in the aggregated state. The high brightness of their aggregates in aqueous solutions enables them to be utilized as fluorescence visualizers for imaging organelles such as mitochondria, cell membrane, lipid droplets and lysosomes.[24–27] So far, most of the AIE probes target an organelle specifically with a single emission colour. Therefore, two or more probes with distinct colours are needed simultaneously to co-stain different organelles. Indeed, it would be fascinating if a single AIE fluorophore can image two or more organelles with distinct emissions. Such a system can simplify the cell manipulation, but until now, no such example has been reported.

In this work, we report the synthesis of a new AIE-active α-cyanostilbene derivative, namely ASCP, and its application in mitochondria and nucleolus imaging. We here demonstrate that ASCP can simultaneously label mitochondria and nucleolus in live cells with distinct fluorescence, high specificity and superior photostability.

2. Experimental section

2.1 Materials

Tetrahydrofuran (THF; Labscan) was distilled from sodium benzophenone ketyl under nitrogen immediately before use. 1,2-Dioleoyl-*sn-glycero*-4-phosphocholine, 1,1′,2,2′-tetraoleoyl cardiolipin (TOCL), 1,2-dioleoyl-*sn-glycero*-3-phospho-L-serine sodium salt, 1,2-dipalmitoleoyl-*sn-glycero*-3-phosphoethanolamine, and L-α-phosphatidylinositol (soy) (sodium salt) were purchased from Avanti Polar Lipids, Inc. *N*-Hexanoyl-D-sphingomyelin (SM) was purchased from Sigma. Minimum essential medium (MEM), phosphate buffered saline (PBS), fetal bovine serum (FBS), sodium dodecyl sulphate (SDS), HEPES buffer, penicillin, streptomycin, MitoTracker Green and SYTO RNASelect were purchased from Invitrogen. DNA, RNA, DNase I and RNase I were purchased from Aldrich.

2.2 Instruments

^{1}H and ^{13}C NMR spectra were measured on a Bruker AV 400 spectrometer in $CDCl_3$ and DMSO-d_6 using tetramethylsilane (TMS; δ = 0) as internal reference. Absorption spectra were measured on a Varian Cary 50 UV-Vis spectrophotometer. Steady-state fluorescence spectra were recorded on a Perkin-Elmer LS 55 spectrofluorometer with xenon discharge lamp excitation. Mass spectra were recorded on a GCT Premier CAB 048 mass spectrometer operated in MALDI-TOF mode. Fluorescence images were collected on an Olympus BX 41 fluorescence microscope. Laser confocal scanning microscope images were collected on a Zeiss laser scanning confocal microscope (LSM7 DUO) and analyzed using ZEN 2009 software (Carl Zeiss).

2.3 Synthesis

ASCP or compound **6** was prepared according to the synthetic route shown in Scheme 1. Detailed procedures are shown below.

Synthesis of compound 3. Into a 100 mL round bottom flask were dissolved 4-bromophenylacetonitrile (**1**; 0.69 g, 3.50 mmol) and 4-(dimethylamino)benzaldehyde (**2**; 0.81 g, 3.00 mmol) in 40 mL ethanol. Sodium hydroxide (0.14 g, 3.50 mmol) in 5 mL ethanol was then added slowly into the mixture. After stirring for 2 h, the pale yellow precipitates were filtered, washed with ethanol and dried under reduced pressure. Yield: 80%. ^{1}H NMR (400 MHz, $CDCl_3$), δ (ppm): 7.86 (d, 2H, J = 8.4 Hz), 7.54–7.48 (m, 4H), 7.38 (s, 1H), 6.73 (d, 2H, J = 8 Hz), 3.07 (s, 6H). HRMS (MALDI-TOF): m/z 326.0217 (M^+, calcd. 326.0419).

Synthesis of compound 5. Into a 100 mL two-necked round bottom flask equipped with a condenser were added **3** (0.10 g, 0.306 mmol), (4-hydroxylphenyl)boronic acid (**4**; 45 mg, 0.387 mmol), potassium carbonate (0.422 g, 3.06 mmol) and $Pd(PPh_3)_4$ (10 mg, 0.01 mmol) in 20 mL THF and 3 mL water under nitrogen. The mixture was stirred and heated to reflux overnight. After cooling to room temperature, the mixture was extracted with dichloromethane (DCM) three times. The organic phase was collected, washed with water and dried over anhydrous sodium sulfate. After solvent evaporation, the crude product was purified by silica-gel column chromatography using DCM/ethyl acetate (v/v = 99 : 1) as an eluent to furnish an orange solid as the product. Yield: 74%. ^{1}H NMR (400 MHz, $CDCl_3$), δ (ppm): 8.68 (d, 2H, J = 4.4 Hz), 7.76–7.68 (m, 4H), 7.55 (d, 2H, J = 4.4 Hz), 7.26 (s, 1H), 6.74 (d, 2H, J = 8.4 Hz), 3.08 (s, 6H). ^{13}C NMR (100 MHz, $CDCl_3$), δ (ppm): 150.7, 149.4, 149.3, 144.6, 142.4, 137.4, 137.5, 131.2, 130.9, 129.2, 127.0, 126.8, 125.4, 120.9, 120.9, 120.7, 111.0, 110.6, 106.0, 39.4, 39.3. HRMS (MALDI-TOF): m/z 325.1575 (M^+, calcd. 325.1579).

Synthesis of compound 6 (ASCP). In a 100 mL two-necked round bottom flask equipped with a condenser was dissolved **5** (50 mg, 0.154 mmol) in 5 mL acetonitrile. Iodomethane (0.1 mL) was then added and the mixture was heated to reflux for 8 h. After cooling to room temperature, the mixture was poured into diethyl ether. The dark red precipitates formed

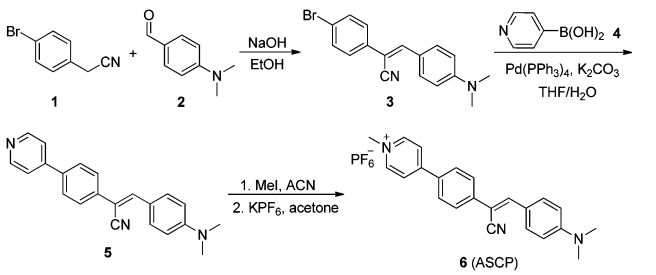

Scheme 1 Synthetic route to ASCP.

were filtered by suction filtration. The precipitates were re-dissolved in acetone and mixed with saturated KPF_6 solution (5 mL). After stirring for 1 h, acetone was evaporated by compressed air. The dark red precipitates were filtered again, washed with water and dried under reduced pressure. Yield: 95%. ^{1}H NMR (400 MHz, DMSO-d_6), δ (ppm): 8.98 (d, 2H, J = 6.8 Hz), 8.53 (d, 2H, J = 6.8 Hz), 8.18 (d, 2H, J = 8.4 Hz), 8.03 (s, 1H), 7.93–7.40 (m, 4H), 6.83 (d, 2H, J = 8.8 Hz), 4.29 (s, 3H), 3.03 (s, 6H). ^{13}C NMR (100 MHz, DMSO-d_6), δ (ppm): 153.0, 152.0, 145.3, 144.4, 138.3, 132.0, 131.6, 128.5, 125.6, 123.5, 120.3, 118.9, 111.4, 100.3, 46.8. HRMS (MALDI-TOF): m/z 340.1826 (M^+, calcd. 340.1814).

2.4 Cell culture

HeLa cells were cultured in MEM supplemented with 10% heat-inactivated FBS, 100 units per mL penicillin and 100 μg mL^{-1} streptomycin, in a humidity incubator with 5% CO_2 at 37 °C. Before experiment, the HeLa cells were pre-cultured until confluence was reached.

2.5 Cytotoxicity study

2-(4,5-Dimethyl-2-thiazolyl)-2,5-diphenyltetrazolium bromide (MTT) assay was used to evaluate the cytotoxicity of ASCP. HeLa cells (provided by American Type Culture Collection) were seeded in a 96-well plate at a density of 5000 cells per well. After 24 h of incubation, the cells were exposed to a series of doses of ASCP (0–10 μM) in culture medium at 37 °C. Eight hours later, 10 μL of freshly prepared MTT solution was added into each well. After further incubation for 4 h, 100 μL of solubilization solution containing 10% SDS and 0.01 M HCl was added to dissolve the purple crystals. Four hours later, the absorbance at 595 nm was recorded using a Perkin-Elmer Victor plate reader. The experiment was performed at least five times.

2.6 Cell imaging

HeLa cells were seeded on a 35 mm Petri dish with a glass cover slide. After overnight cell culture, the HeLa cells were incubated in an aqueous solution of ASCP (5 μM) for 30 min or SYTO RNASelect (500 nM) for 20 min. The dye-labelled cells were washed with fresh phosphate buffered saline (PBS; pH 7.4) three times before fluorescence imaging. For co-staining experiments, a solution of MitoTracker Green (MTG; 200 nM) was added to the HeLa cells incubated with an aqueous solution of ASCP for 15 min. After further incubation for 15 min, the dye-labelled cells were washed with fresh PBS solution three times and then imaged using wide-field fluorescence and confocal microscopes.

2.7 Preparation of lipid vesicles

Chloroform stocks of different lipids (10 mg mL^{-1}) were mixed in a desired molar ratio and dried under a stream of nitrogen. The lipid films were hydrated in 25 mM HEPES buffer (pH 7.4) to a final lipid concentration of 2.2 mM. The lipid mixtures were incubated for 30 min at 37 °C and then sonicated for 1 h. The lipid vesicles were obtained by extruding 11 times through a 100 nm pore size polycarbonate filter at 50 °C on a pre-warmed lipid extruder.[28,29]

2.8 DNase and RNase digest tests

HeLa cells were fixed by 4% paraformaldehyde for 30 min. After incubation with 1% Triton X-100 for 2 min, the cells were permeabilized and rinsed with PBS twice. The cells were incubated with either ASCP (10 μM) or SYTO RNASelect (5 μM) solution for 30 min. After washing with PBS twice, a PBS solution (100 μL) mixed with DNase (30 μg mL^{-1}) or RNase (25 μg mL^{-1}) was added and the cells were incubated in an incubator with 5% CO_2 at 37 °C for 2 h. The cells were rinsed with PBS twice before imaging using a wide-field fluorescence microscope.

2.9 Photostability test

Dye-labelled live HeLa cells were imaged on a confocal microscope. Conditions: excitation wavelength: 560 nm and emission filter: 650–750 nm (ASCP); excitation wavelength: 488 nm and emission filter: 500–600 nm (SYTO RNASelect).

3. Results and discussion

3.1 Design and synthesis of ASCP

Tetraphenylethene (TPE) and its derivatives are archetypal AIE luminogens (AIEgens). Because of their efficient emission in the aggregated state, they have been utilized as fluorescent agents for bioimaging with high sensitivity and photostability. By incorporation of a pyridinium (Py) unit to TPE, the resultant AIEgen can visualize mitochondria in HeLa cells with high specificity and bright yellow emission. To minimize the interference from autofluorescence, fluorophores with longer wavelength excitation and emission are more desirable. On the other hand, α-cyanostilbene is a good building block for generating AIEgens with different emissions by attaching various donor groups to its molecular structure. Through molecular engineering, a new AIEgen, namely ASCP, was designed. This luminogen consisted of three components: (1) α-cyanostilbene as the AIE skeleton and the linker; (2) the dimethylamino group as the donor to tune the emission to the red region; and (3) Py salt as the targeting agent for mitochondria. Its synthetic procedure is described in Scheme 1. Compound **3** was synthesized by Knoevenagel condensation of 4-bromophenylacetonitrile (**1**) and 4-(dimethylamino)benzaldehyde (**2**) under basic conditions. Suzuki coupling of **3** with (4-hydroxylphenyl)boronic acid (**4**) in the presence of $Pd(PPh_3)_4$ and K_2CO_3 afforded **5**. Treatment of **5** with iodomethane and KPF_6 finally furnished the desirable product ASCP in high yield. The detailed synthesis and characterization of ASCP and the intermediates are given in the Experimental section and Fig. S1–S8 in the ESI.†

3.2 Optical properties

We first studied the optical properties of ASCP. Due to the hydrophilic nature of the Py salt, ASCP is soluble in polar solvents, slightly soluble in water but insoluble in nonpolar solvents such as dioxane and toluene. ASCP exhibits an absorption band at around 450 nm, irrespective of the type of solvent used (Fig. 1A). In contrast, it shows obvious different emission

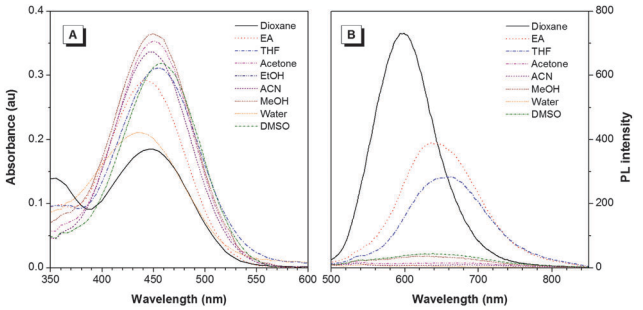

Fig. 1 (A) Absorption spectra and (B) emission spectra of ASCP in different solvents. Concentration: 10 μM; λ_{ex} = 460 nm.

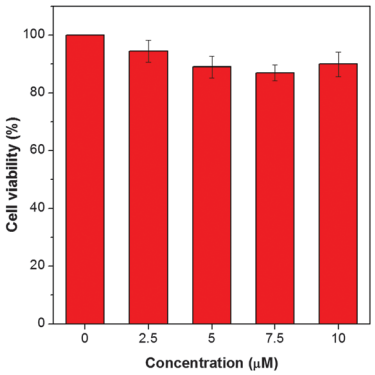

Fig. 3 Viability of HeLa cells in the presence of different concentrations of ASCP for 8 h. Data are expressed as the mean value of five separate trials.

colours and intensities when the measurement was carried out in different solvents (Fig. 1B).

ASCP emits strong orange light in dilute dioxane solution. Owing to the twisted intramolecular charge transfer (TICT) effect,[30] the emission of the dye molecule weakened and red-shifted with increasing solvent polarity. In dilute DMSO solution, ASCP shows a faint red fluorescence. In contrast, gradual addition of toluene to its DMSO solution enhanced the light emission and changed the emission colour to orange due to the gradual decrement of the solvent polarity (Fig. 2). At high toluene fraction, a much rapid fluorescence enhancement was observed due to the formation of ASCP aggregates along with the activation of the AIE process.

3.3 Cell imaging

The strong emission of ASCP in the aggregated state encourages us to utilize it as a fluorescence visualizer for mitochondrion imaging. To examine whether the dye is suitable for bio-imaging, the cytotoxicity of ASCP on HeLa cells was first evaluated using MTT assay. As depicted in Fig. 3, the cell viability remains high at ASCP concentrations as high as 10 μM, suggesting that ASCP possesses good biocompatibility. ASCP was first assessed for its capability to stain specific organelles in live HeLa cells. The HeLa cells were cultured and incubated in MEM with 5 μM ASCP for 30 min. The cells were washed with fresh PBS and then observed under a fluorescence microscope. Thanks to the high specificity of the Py unit in ASCP, the reticulum structures of mitochondria are stained with intense orange emission (Fig. 4A). To further validate the specificity of ASCP, MitoTracker Green (MTG), a commercial mitochondrial imaging agent, was used to co-stain the HeLa cells. The cell images acquired on a confocal microscope illustrate that the orange fluorescence from ASCP has an excellent correlation (96.4%) with the green emission of MTG (Fig. 4D–F).

Surprisingly, by altering the focus, red fluorescence was observed in the nucleolus (Fig. 4B). Thus, it seems that the two distinct fluorescence observed from mitochondria and nucleolus is correlated with the specific interactions of ASCP with different biomolecules.

The most abundant components in mitochondria and nucleolus are phospholipids and nucleic acids (DNAs and RNAs), respectively. To examine our hypothesis, phospholipids found in the mitochondrial membrane (Chart S1, ESI†) and nucleic acids were chosen for mimicking the actual intracellular environment. Different lipid vesicles were first fabricated as models of mitochondria by mixing the desired ratio of phospholipids.

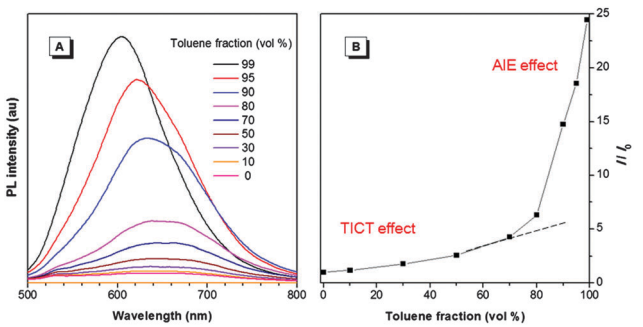

Fig. 2 (A) Emission spectra of ASCP in toluene/DMSO mixtures with different toluene fractions (f_t). (B) Plot of relative emission intensity (I/I_0) at 650 nm *versus* the composition of the toluene/DMSO mixture of ASCP. I_0 = emission intensity of ASCP in pure DMSO solution. Concentration: 10 μM; λ_{ex} = 460 nm.

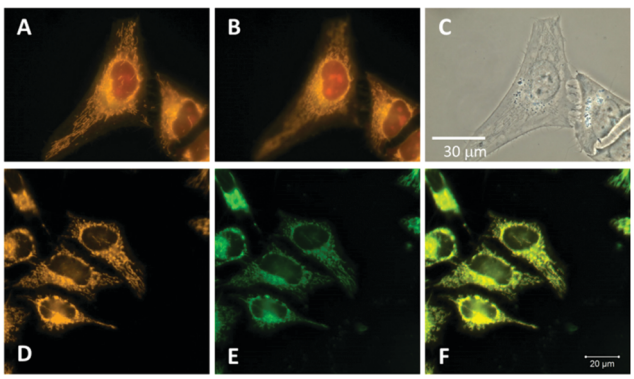

Fig. 4 (A and B) Fluorescence and (C) bright-field images of HeLa cells stained with ASCP (5 μM) for 30 min with focus at mitochondria (A) and nucleolus (B), respectively. λ_{ex} = 460–490 nm; scale bar = 30 μm. (D and E) Confocal images of HeLa cells stained with (D) ASCP (5 μM) and (E) MitoTracker green (MTG; 200 nM). (F) The merged image of (D) and (E). Conditions: λ_{ex} = 405 nm and λ_{em} = 600–700 nm for ASCP; λ_{ex} = 488 nm and λ_{em} = 500–540 nm for MTG; scale bar = 20 μm.

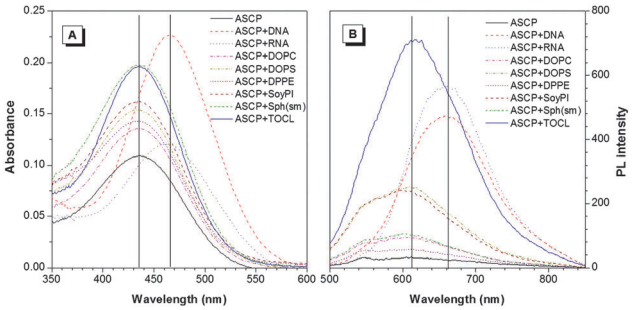

Fig. 5 (A) Absorption spectra and (B) emission spectra of ASCP mixed with different phospholipid vesicles, DNA and RNA in HEPES (pH 7.4) buffer solutions with 1% DMSO. Concentration: 10 μM; λ_{ex} = 460 nm.

The absorption and emission spectra of ASCP in the presence of lipid vesicles and nucleic acids in HEPES were then recorded. ASCP exhibits an absorption maximum at 435 nm in HEPES, showing no or little wavelength shift when treated with lipid vesicles. On the other hand, the absorption maximum of ASCP is red-shifted by 20 nm in the presence of nucleic acids (Fig. 5A). Similarly, while a 50 nm bathochromic shift in the emission maximum was observed when ASCP was mixed with nucleic acids, no change in the ASCP emission was observed for lipid vesicles (Fig. 5B). These results are consistent with the observations from fluorescence images as shown in Fig. 4A and B.

It becomes clear why ASCP exhibits two different fluorescence in mitochondria and nucleolus. The next question is whether it is possible to use ASCP to collect individual fluorescence from mitochondria and nucleolus without cross contamination. To answer this, we attempted to collect the confocal images of dye-labelled HeLa cells by changing the excitation wavelengths and the emission filters. After optimizing the conditions, mitochondria can be visualized individually as orange fluorescence under 405 nm light excitation (Fig. 6A). On the other hand, only red fluorescence was observed in nucleoli at an excitation wavelength of 560 nm (Fig. 6B).

3.4 Origin of fluorescence in nucleolus

Intercalation and electrostatic attraction are the possible interactions between ASCP and nucleic acids. When ASCP enters the cavities of nucleic acids, it may adopt a more co-planar and conjugated conformation, and hence shows a redder emission. On the other hand, the hydrogen bonds between the nucleotides in nucleic acids may provide a relatively polar environment for

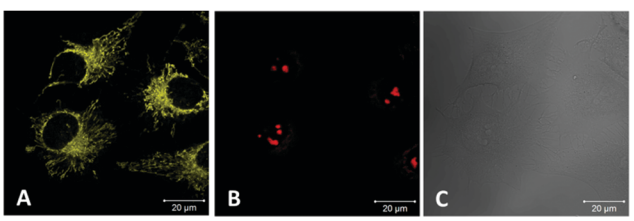

Fig. 6 (A and B) Confocal and (C) bright field images of HeLa cells stained with ASCP (5 μM) for 30 min. Conditions: (A) λ_{ex} = 405 nm; λ_{em} = 500–650 nm; (B) λ_{ex} = 560 nm; λ_{em} = 650–750 nm.

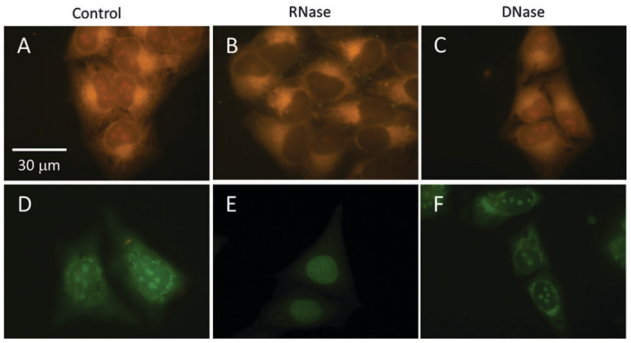

Fig. 7 Fluorescence images of HeLa cells stained with (A–C) ASCP (10 μM) for 2 h and (D–F) SYTO RNASelect (5 μM) for 2 h with or without treatment with RNase or DNase.

ASCP to emit at the longer wavelength region. In order to gain a better understanding of the origin of red fluorescence, fluorescence imaging experiments were performed after the ASCP-labelled cells were fixed and treated with deoxyribonuclease (DNase) and ribonuclease (RNase). From the fluorescence images shown in Fig. 7, the specificity of ASCP to the nucleolus was lost when RNase was applied (Fig. 7B). However, the dye-labelled cells are still emissive after treated with DNase (Fig. 7C). The performance of ASCP was further verified by using SYTO RNASelect, a commercial fluorescent probe for nucleolus. As shown in Fig. 7E and F, SYTO RNASelect performed similar to ASCP. Since RNA is the major constituent in the nucleolus, both ASCP and SYTO RNASelect tend to accumulate in nucleolus due to the strong electrostatic attraction. When the dye-labelled cells are treated with RNase, the binding sites for intercalation collapsed and the dye molecules are no longer bound to the RNA fragments. Thus, the fluorescence emission of ASCP and SYTO RNASelect in RNA-rich nucleolus is decreased dramatically.

3.5 Photostability

Photostability is a critically important parameter for a fluorescent probe to find promising application in organelle imaging and tracking. To quantitatively investigate the photobleaching resistance of ASCP and SYTO RNASelect, continuous scanning

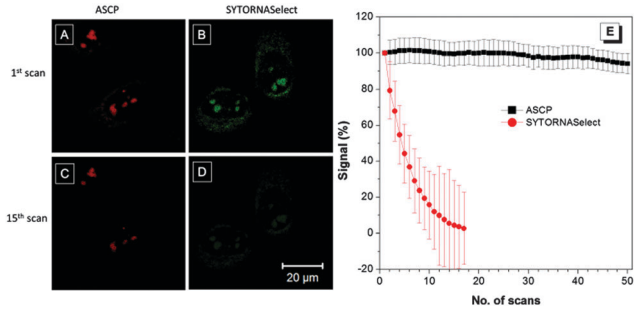

Fig. 8 Confocal images of HeLa cells stained with (A and C) ASCP and (B and D) SYTO RNASelect acquired under continuous excitation. (E) Signal (%) of fluorescence emission of (black) ASCP and (red) SYTO RNASelect of different numbers of scan. Conditions: λ_{ex} = 560 nm and λ_{em} = 650–750 nm for ASCP; λ_{ex} = 488 nm, λ_{em} = 500–600 nm for SYTO RNASelect.

of the dye-labelled cells by laser irradiation was carried out and the fluorescence signal at each scan was recorded. The dye-labelled cells were irradiated at 560 and 488 nm, respectively, with the same power. As shown in Fig. 8, 5% fluorescence loss was observed in ASCP-stained cells after 50 scans. In contrast, almost no fluorescence signal was detected from the cells stained with SYTO RNASelect after 15 scans. This result suggests that ASCP possesses higher photo-bleaching resistance or photostability than SYTO RNASelect.

4. Conclusions

In summary, a dual-color organelle-specific probe with the AIE feature for mitochondria and nucleolus is developed. Due to the different interactions with mitochondrial membrane and nucleic acids, distinct emission colors from mitochondria and nucleolus are observed under a fluorescence microscope. Owing to its high brightness, excellent biocompatibility and superior photostability, the AIE fluorescent probe is a promising candidate for the simultaneous imaging of mitochondria and nucleolus. Further studies on the development of AIEgens with multi-organelle-specific emissions and exploration of their biomedical applications are ongoing in our laboratory.

Acknowledgements

This work was partially supported by the National Basic Research Program of China (973 Program, 2013CB834701 and 2013CB834702), the University Grants Committee of Hong Kong (AoE/P-03/08), the Research Grants Council of Hong Kong (16301614, 16305015 and N_HKUST604/14), the Innovation and Technology Commission (ITC-CNERC14SC01). We thank the support of the Guangdong Innovative Research Team Program (201101C0105067115).

Notes and references

1 M. M. Yusupov, G. Z. Yusupova, A. Baucom, K. Lieberman, T. N. Earnest, J. H. D. Cate and H. F. Noller, *Science*, 2001, **292**, 883.
2 Y. W. Lam, L. Trinkle-Mulcahy and A. I. Lamond, *J. Cell Sci.*, 2005, **118**, 1335.
3 M. O. J. Olson, K. Hingorani and A. Szebeni, *Int. Rev. Cytol.*, 2002, **219**, 199.
4 M. Carmo-Fonseca, L. Mendes-Soares and I. Campos, *Nat. Cell Biol.*, 2000, **2**, E107.
5 D. Hernandez-Verdun, P. Roussel and J. Gébrane-Younès, *J. Cell Sci.*, 2002, **115**, 2265.
6 A. K. L. Leung, J. S. Andersen, M. Mann and A. I. Lamond, *Biochem. J.*, 2003, **376**, 553.
7 U. Scheer and R. Hock, *Curr. Opin. Cell Biol.*, 1999, **11**, 385.
8 R. Parlato and B. Liss, *Biochim. Biophys. Acta*, 2014, **1842**, 791.
9 S. Boulon, B. J. Westman, S. Hutten, F. M. Boisvert and A. I. Lamond, *Mol. Cell*, 2010, **40**, 216.
10 I. Johnson and M. T. Z. Spence, *Molecular probes handbook, A guide to fluorescent probes and labeling technologies*, Invitrogen, 11th edn, 2010, ch. 8, p. 314.
11 D. Honcharenko, C. Zhou and J. Chattopadhyaya, *J. Org. Chem.*, 2008, **73**, 2829.
12 C. A. Alabi, K. T. Love, G. Sahay, T. Stutzman, W. T. Young, R. Langer and D. G. Anderson, *ACS Nano*, 2012, **6**, 6133.
13 Y. Kam, A. Rubinstein, A. Nissan, D. Halle and E. Yavin, *Mol. Pharmaceutics*, 2012, **9**, 685.
14 P. J. Santangelo, B. Nix, A. Tsourkas and G. Bao, *Nucleic Acids Res.*, 2004, **32**, e37.
15 J. S. Paige, K. Y. Wu and S. R. Jaffrey, *Science*, 2011, **333**, 642.
16 G. Bao, J. R. Won and A. Tsourkas, *Annu. Rev. Biomed. Eng.*, 2009, **11**, 25.
17 I. E. Catrina, S. A. E. Marras and D. P. Bratu, *ACS Chem. Biol.*, 2012, **7**, 1586.
18 P. Santangelo, N. Nitin and G. Bao, *Ann. Biomed. Eng.*, 2006, **34**, 39.
19 Q. Li, Y. Kim, J. Namm, A. Kulkarni, G. R. Rosania, Y. H. Ahn and Y. T. Chang, *Chem. Biol.*, 2006, **13**, 615.
20 G. Song, Y. Sun, Y. Liu, X. Wang, M. Chen, F. Miao, W. J. Zhang, X. Yu and J. Jin, *Biomaterials*, 2014, **35**, 2103.
21 J. T. Miao, C. Fan, R. Sun, Y. J. Xu and J. F. Ge, *J. Mater. Chem. B*, 2014, **2**, 7065.
22 M. Filosto, M. Scarpelli, M. S. Cotelli, V. Vielmi, A. Todeschini, V. Gregorelli, P. Tonin, G. Tomelleri and A. Padovani, *J. Neurol.*, 2011, **258**, 1763.
23 A. Johri and M. F. Beal, *J. Pharmacol. Exp. Ther.*, 2012, **342**, 619.
24 N. Zhao, M. Li, Y. Yan, J. W. Y. Lam, Y. L. Zhang, Y. S. Zhao, K. S. Wong and B. Z. Tang, *J. Mater. Chem. C*, 2013, **1**, 4640.
25 M. Gao, Q. Hu, G. Feng, B. Z. Tang and B. Liu, *J. Mater. Chem. B*, 2014, **2**, 3438.
26 Y. Li, Y. Wu, J. Chang, M. Chen, R. Liu and F. Li, *Chem. Commun.*, 2013, **49**, 11335.
27 Q. Hu, M. Gao, G. Feng, X. Chen and B. Liu, *ACS Appl. Mater. Interfaces*, 2015, **7**, 4875.
28 C. W. T. Leung, Y. Hong, J. Hanske, E. Zhao, S. Chen, E. V. Pletneva and B. Z. Tang, *Anal. Chem.*, 2014, **86**, 1263.
29 D. R. Voelker, *Biochemistry of lipids, Lipoproteins and Membranes*, 4th edn, 2002, ch. 17.
30 R. Hu, E. Lager, A. Aguilar-Aguilar, J. Liu, J. W. Y. Lam, H. H. Y. Sung, I. D. Williams, Y. Zhong, K. S. Wong, E. Pena-Cabrera and B. Z. Tang, *J. Phys. Chem. C*, 2009, **113**, 15845.